A Flight Dynamics Investigation of Compound Helicopter Configurations

Kevin Ferguson
k.ferguson.1@research.gla.ac.uk
Ph.D Student
University of Glasgow
Glasgow, United Kingdom

Douglas Thomson
Douglas.Thomson@glasgow.ac.uk
Senior Lecturer
University of Glasgow
Glasgow, United Kingdom

ABSTRACT

Compounding has often been proposed as a method to increase the maximum speed of the helicopter. There are two common types of compounding known as wing and thrust compounding. Wing compounding offloads the rotor at high speeds delaying the onset of retreating blade stall, hence increasing the maximum achieveable speed, whereas with thrust compounding, axial thrust provides additional propulsive force. The concept of compounding is not new but recently there has been a resurgence of interest in the configuration due to the emergence of new requirements for speeds greater than those of conventional helicopters. The aim of this paper is to investigate the dynamic stability characteristics of compound helicopters and compare the results with a conventional helicopter. The paper discusses the modelling of two compound helicopters, with the first model featuring a coaxial rotor and pusher propeller. This configuration is known as the coaxial compound helicopter. The second model, known as the hybrid compound helicopter, features a wing and two propellers providing thrust compounding. Their respective trim results are presented and contrasted with a baseline model. Furthermore, using a numerical differentiation technique, the compound models are linearised and their dynamic stability assessed. The results show that the frequency of the coaxial compound helicopter's dutch roll mode is less than that of the baseline helicopter and there is also greater roll damping. With regards to the hybrid compound helicopter the results show greater heave damping and the stabilisation of the phugoid due to the addition of the wing and propellers.

NOTATION

$\mathbf{f}$	forcing vector function
g	acceleration due to gravity (m/s)
u, v, w	translational velocities (m/s)
$\mathbf{u}$	control vector
v_0	uniform induced velocity component (m/s)
$\mathbf{x}$	state vector
$\mathbf{x}_{\text{prop}}$	position of the propeller hub (m)
$\mathbf{A}, \mathbf{B}$	stability and control matrices
C_q, C_t	torque and thrust coefficient
C_{t_u}, C_{t_l}	upper and lower rotor thrust coefficient
I_β	flap moment of inertia (kgm^2)
K_β	centre-spring rotor stiffness (Nm/rad)
L_p	roll damping derivative (1/s)
L_v	dihedral derivative (rad/ms)
M_q	pitching damping derivative (1/s)
M_u	speed stability derivative (1/s)
N_b	number of rotor blades
N_p	yawing moment due to roll rate (1/s)
P	coaxial rotor power (HP)
R, R_{prop}	radius of the main rotor and propeller blade (m)
U_e	forward speed at trim (m/s)
U_p	normal velocity of a rotor blade element (m/s)
U_t	tangential velocity of a rotor blade element (m/s)
X_{port}, X_{star}	port and starboard propeller thrust (N)
X_u	drag damping derivative (1/s)
Z_w	heave damping derivative (1/s)
α_w	angle of attack of a wing element (rad)
γ	Lock number
γ_s	rotor shaft tilt (rad)
λ_l,λ_u	non-dimensional lower and upper rotor inflow
μ	non-dimensional advance ratio
μ_z	non-dimensional normal velocity of the rotor hub
ω	frequency (rad/s)
ω_{dr}	dutch roll mode frequency (rad/s)
Ω , Ω_{prop}	main rotor and propeller rotational speed (rad/s)
ϕ, θ	Euler angles (rad)
ϕ_i	rotor inflow angle (rad)
σ,σ_{prop}	rotor and propeller solidity
θ_{fixed}	fixed wing pitch incidence (rad)
θ_{diff}	differential collective (rad)
θ_l, θ_u	lower and upper rotor collective pitch (rad)
θ_{port}, θ_{star}	port and starboard propeller collective (rad)
θ_{prop}	coaxial propeller collective setting (rad)
$\bar{\theta}_{\text{prop}}$	mean collective setting of the two propellers (rad)
θ_{tw}	gradient of linear twist (rad)
θ_0	main rotor collective pitch angle (rad)
$\bar{\theta}_0$	mean upper and lower rotor collective pitch (rad)
θ_{1s},θ_{1c}	longitudinal and lateral cyclic pitch (rad)

Presented at the AHS 69th Annual Forum, Phoenix, Arizona, May 21–23, 2013.

INTRODUCTION

The compound helicopter has experienced a resurgence of interest recently due to its ability to obtain speeds that significantly surpass the conventional helicopter. This increase in speed would make the compound helicopter suitable for various roles and missions such as troop insertion, search and rescue, ship replenishment as well as short haul flights in the civil market. The compounding of a helicopter is not a new idea but the development of a compound helicopter has proven elusive for the rotorcraft community due to a combination of technical problems and economical issues (Ref. 1). The rotorcraft community is again exploring the compound helicopter design, with Sikorsky and Eurocopter both testing their prototypes. The Sikorsky helicopter, the Sikorsky X2, is a coaxial design with thrust compounding whereas the Eurocopter helicopter, the Eurocopter X^3, is a conventional single rotor machine with both thrust and wing compounding.

The maximum speed of a conventional helicopter is restricted due to aerodynamic limitations, installed engine power and airframe drag (Ref. 2). The problems associated with installed engine power and airframe drag can be minimised through careful design, but the main factor limiting the maximum speed of the helicopter is retreating blade stall. The compound helicopter is designed to delay the flight speed at which the condition of retreating blade stall occurs thereby increasing the maximum operating speed of the vehicle. Both the Sikorsky X2 and the Eurocopter X^3 have different methods to avoid retreating blade stall until higher speeds. The X2, with its coaxial rotor, uses the ABC (Advancing Blade Concept) rotor system to offload the retreating side of the disc at high speeds and therefore avoid blade stalling. This concept was originally developed in the 1960s but the aircraft never entered production (Ref. 3). Recently, the ABC rotor system has been revisited and the design improved upon with the use of advanced aerofoil sections and active vibration control (Refs. 4, 5). Due to these improvements as well as the pusher propeller providing an extra component of axial thrust, the Sikorsky X2 is able to reach speeds of 250 knots (Ref. 6).

In contrast, the wings of the Eurocopter X^3 offload the rotor at high speeds and the propellers provide the propulsive force to overcome the fuselage drag. Recent publications have reported that the Eurocopter X^3 is able to reach a maximum speed of 232 knots. It is therefore evident that these helicopters are capable of greater speeds than their conventional counterparts.

As mentioned previously, the compounding of the helicopter is not a novel idea. There have been various flight test programmes that have investigated the compound helicopter configuration (Refs. 7–10). Although these programmes never led to a production vehicle, they did provide some insight into the problems that designers may face with the development of a compound helicopter. One issue is the inherent control redundancy that results from compounding the conventional configuration. The compounding results in an additional control relative to a conventional helicopter and therefore there is an issue on how to integrate this control into the vehicle. The Rotor Systems Research Aircraft (RSRA) conducted a series of flight tests which featured a fixed setting of collective pitch (Ref. 7). This set-up offers a reduction in terms of pilot workload but does not fully exploit the additional control offered by compounding. A successful compound helicopter would require a control system that exploits the additional control to enhance the performance benefits that compounding offers without significantly increasing pilot workload. Another issue that arose from the flight test programme of the XH-51A helicopter (Ref. 8) was the tendency of the rotor to overspeed. During high speed manoeuvres the load factor of the main rotor increased quicker than that of the wing thus resulting in rotor overspeed. The AFCS would have to reduce the collective pitch setting of the main rotor in high speed manoeuvres, thereby avoiding rotor overspeed. The Lockheed Cheyenne, another notable compound helicopter, encountered problems with its gyro design which led to a fatal crash (Ref. 9). The combination of this crash, other problems with the design and political issues ended the Cheyenne programme despite exhibiting excellent performance. It is clear that the compounding of a helicopter presents some problems, all of which will have to be overcome, or at least ameliorated, but the advantages, in terms of increasing the maximum speed of the helicopter are clear.

More recently, Orchard et al. focused on the design of the compound helicopter (Ref. 11). Their study investigated the various design aspects of a compound helicopter such as the wing, rotor and propulsor design. The study suggests that a medium size wing should be used to provide a compromise between the beneficial effect of offloading the rotor at high speeds and the adverse effect of creating aerodynamic download at low speeds. To optimise the compound design, most authors agree that a wing must be supplemented with auxiliary propulsion (Refs. 12–15). The reason for this is that a wing-only compound helicopter tends to have a more pitch down attitude, relative to a baseline helicopter (Ref. 12). In forward flight, the wing offloads the main rotor and therefore reduces the rotor thrust. The rotor thrust is still required to overcome the fuselage drag as well as the additional drag of the wing, hence to trim the helicopter the smaller rotor thrust vector must be tilted more forward to provide the propulsive force. As a result, the pitch of the helicopter tends to be more nose down than that of the baseline configuration which reduces the angle of attack of the wing and therefore its lifting capability. However, if auxiliary propulsion is introduced the pitch attitude can be controlled, therefore fully exploiting the lifting capability of the wing. An alternative approach to increasing the maximum speed of the helicopter is the 1950's Gyrodyne concept that was recently revisited by Houston (Ref. 16). The Gyrodyne concept employs a propulsor mounted onto a side of the fuselage to replace the tail rotor and therefore fulfil the dual role of providing axial thrust and the anti-torque moment. Houston used the Puma SA330 helicopter in his study and showed that this Gyrodyne set-up increased the maximum speed of the helicopter by 50 knots.

It is clear that there is no shortage of literature concerning the compound configuration, all of which confirms the po-

tential advantages of the vehicle. The next logical question relates to the dynamic stability of this aircraft class, and its effect on flying qualities and control. The main aim of this paper is to assess the dynamic stability of compound helicopters and compare their stability to a conventional helicopter. The strategy for the current work is to use an established mathematical model of a conventional helicopter (in this case the AgustaWestland Lynx), then convert this model to represent compound configurations. The Lynx was chosen as a well established data set (Ref. 17) and model was available (Ref. 18). The compound configurations that are examined in the paper are similar to the Sikorsky X2 and Eurocopter X^3. The first compound model is referred to as the Coaxial Compound Helicopter (CCH) Model which features a coaxial rotor and a pusher propeller as seen in Figure 1. The second model is

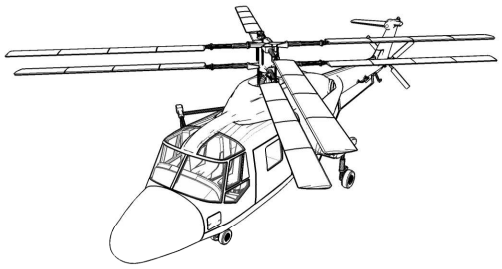

Fig. 1. Sketch of the Coaxial Compound Helicopter (CCH) Model

known as the Hybrid Compound Helicopter (HCH) model which features a wing and two propellers, as seen in Figure 2. These two compound models are changed as little as possible, relative to the baseline model, to allow for a fair and direct comparison between the results of the compound configurations and the baseline (BL) model. Therefore, unless stated, the design features of the compound helicopter models are identical to that of the conventional Lynx helicopter. The result is two rather unusual looking vehicles, Figures 1 and 2, however it should be stressed that this is not a design exercise, and so to ensure that the effects of compounding are isolated from other factors, the basic vehicle shape and size is maintained.

METHODOLOGY

The compound helicopter models are built using the Helicopter Generic Simulation (HGS) model (Refs. 17, 18). The HGS model is a conventional disc-type rotorcraft model, as described by Padfield (Ref. 17), and has found extensive use in studies of helicopter flight dynamics. The HGS package features multi-blade representations of the main and tail rotor, with each blade assumed to be rigid and of constant chord.

Fig. 2. Sketch of the Hybrid Compound Helicopter (HCH) Model

The rotor lift is assumed to be a linear function of the local blade angle and the drag is modelled using the blade section lift coefficient. The flow is assumed steady and incompressible. The forces and moments of the tailplane, fuselage and fin are calculated using a series of look-up tables which are a function of the local aerodynamic angles. The HGS package was designed for a conventional helicopter simulation. Therefore models of a coaxial rotor, propeller and wing are missing from the package. The following section provides an overview these models.

Coaxial Rotor Model

The coaxial rotor is modelled by using two multi-blade rotor models spaced vertically apart. The upper rotor rotates in an anti-clockwise direction (when viewed from above) whereas the lower rotor rotates in a clockwise direction. The dynamic inflow model currently used in the conventional rotor model is adapted to model the inflow of a coaxial configuration. Various coaxial inflow models have been created with Leishman et al. (Refs. 19,20) developing a coaxial inflow model by slightly adapting the classical blade element momentum approach. The results showed very good agreement with experimental results in the hover and in axial flight. Kim and Brown used another approach, using the vorticity transport model (VTM) to model the performance of a coaxial rotor (Refs. 21, 22). Due to the higher fidelity model of the VTM, the performance results mirror the experimental results very closely. The HGS rotor model is developed using a blade element approach and therefore it seems natural to slightly adapt this approach to model the coaxial rotor inflow. Hence, a similar inflow model to that of Leishman's et al., with a few adaptations, is used to model the coaxial rotor inflow. The first assumption made in the development of the coaxial inflow model is that the inflow of the lower rotor does not affect the upper rotor's ability to generate thrust. The second assumption is that the rotors are sufficiently close together that the wake from the upper rotor does not contract radially inward and does not fully develop. This assumption can be made as it assumed that the rotor is

similar to that of the ABC rotor, featuring very stiff blades with a small separation distance between the rotors. Hence the relationship between the rotor thrust and the induced velocity of the upper rotor is

$$C_{t_u} = \lambda_u \sqrt{\mu^2 + (\mu_z - \lambda_u)^2} \tag{1}$$

The lower rotor's inflow consists of a combination of its own induced velocity and the upper rotor's induced velocity. A similar approach was previously used by Sikorsky (Ref. 23) and showed good agreement with experimental results. The inflow equation for the lower rotor is

$$C_{t_l} = 2\lambda_l \sqrt{\mu^2 + (\mu_z - (\lambda_l + \lambda_u))^2} \tag{2}$$

Validation of the Coaxial Rotor Model In order to gain confidence in the coaxial rotor model, the model is compared against "rotor 1" of Harrington's coaxial experimental results (Ref. 24). Harrington's "rotor 1" is a two bladed, untwisted rotor with a solidity of 0.054, rotor radius of 3.81m and a separation distance of 9.5% of the rotor diameter. The HGS rotor model is configured to match Harrington's coaxial arrangement and trimmed in the hover state for various thrust coefficients. Figure 3 compares the thrust and torque coefficients of the coaxial model to that of Harrington's experimental results at a rotational speed of 392 ft/s. Also shown in the figure are the results produced by two rotors acting in isolation. These two isolated rotors significantly over predict the thrust and torque produced by the rotor system. However, the results from the coaxial inflow model compare favourably with the experimental results.

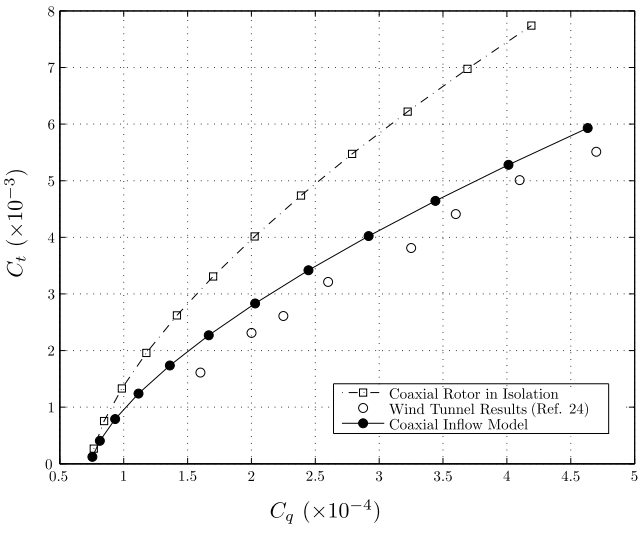

Fig. 3. Validation of the Coaxial Rotor Model in Hover

Moreover, the coaxial rotor model is compared to performance data of a coaxial rotor in forward flight that was obtained experimentally by Dingeldein (Ref. 25). The rotors used in the experiment were identical to that of Harrington's "rotor 1" and the power of the rotor system was measured for various advance ratios. The coaxial rotor system is trimmed for various flight speeds with Figure 4 showing the comparison between Dingeldein's results and the coaxial rotor model. Between advance ratios of 0.1 and 0.2 the coaxial rotor model under predicts the power requirements of the coaxial rotor. As the forward speed increases the wakes of the two rotors begin to skew back (Ref. 26) and a portion of the upper rotor's wake is not ingested into the lower rotor. This effect is not modelled in the current coaxial rotor model and offers an explanation between the discrepancies with the experimental results. However, the results from the coaxial rotor model do follow the same form as Dingeldein's experimental results and the results appear to come closer as forward speed increases. The coaxial rotor model appears to compare well with experimental results, particularly at hover and high speeds. This validation gives confidence to the worth of the coaxial rotor results, although a full validation is not possible due to the lack of experimental data.

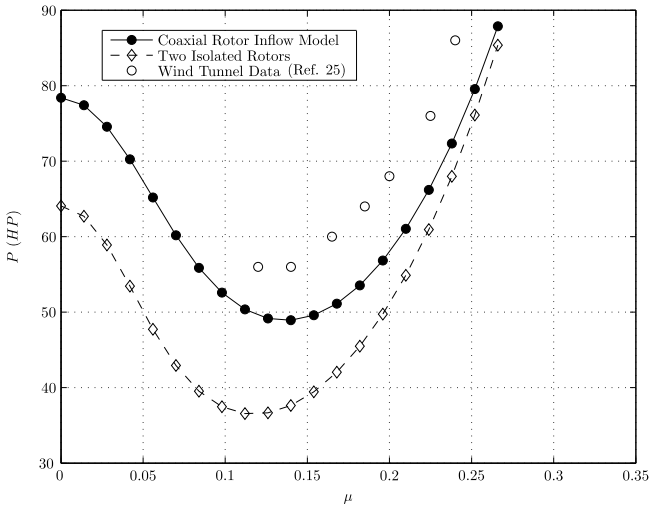

Fig. 4. Validation of the Coaxial Rotor Model in Forward Flight

Propeller Model

Although it would have been convenient simply to use the existing HGS tail rotor model (re-configured to represent a propeller), there are some fundamental issues. In the derivation of the multi-blade representation of the tail rotor various assumptions are made to cast the equations in closed loop form which are not suitable for a propeller. One of these assumptions is that the magnitude of the tangential velocity of a blade element is much greater than that of the normal velocity. This is suitable for edgewise flow and allows for a small angle assumption, namely that the inflow angle ϕ_i becomes

$$\phi_i = \tan^{-1}\left(\frac{U_p}{U_t}\right) \approx \frac{U_p}{U_t} \tag{3}$$

However, for a propeller this assumption only holds true in low speed flight. In high speed flight the normal velocity, U_p, is composed of the forward flight velocity, therefore the tangential and normal velocities are of similar magnitude violating the small angle assumption. To avoid this an individual propeller blade model was created. The development of the model is very similar to that of the tail rotor with the exception that the loads are calculated through numerical integration and no small angle assumptions are made. Like the main and tail rotor models, the airflow over each blade element is assumed to be two dimensional. The blade element forces and moments are integrated across the propeller span and then around the azimuth to calculate the average forces and moments a propeller blade produces per revolution. These forces and moments are then multiplied by the number of blades to calculate the total forces and moments that the full propeller system produces. Again, like the main and tail rotor models, a dynamic inflow model is used to calculate the induced velocities at each blade element.

Wing Model

A simple 2-D representation of the wing using conventional strip theory is used (Ref. 27). With the wing located in the vicinity of the main rotor it is necessary to take into account the rotor's wake in the calculation of the incidence of each wing element (Ref. 28). The assumption in this wing model is that the induced velocity of the rotor wake does not fully develop when it passes over the wing. The angle of attack at the quarter chord position of each wing element, in body axes is therefore

$$\alpha_w = \theta_{\text{fixed}} + \tan^{-1}\left(\frac{w_w - v_0}{u_w}\right) \tag{4}$$

The local angle of attack of each wing element is then used to calculate the aerodynamic coefficients. The loads are numerically integrated across the wing span to calculate the total forces and moments that the wing produces.

COAXIAL COMPOUND CONFIGURATION

Preliminary Design of the Coaxial Compound Helicopter

The coaxial rotor is sized similarly to that of the ABC rotor used on the XH-59A helicopter (Ref. 29). The ABC coaxial rotor features very stiff rotor blades (Ref. 30) to reduce the vertical separation between the rotors and therefore ensure a compact design. A large vertical separation creates some issues by exposing the shaft and control linkages resulting in an increase in parasitic drag at high speeds. Another concern is that a large separation distance would result in the upper rotor creating excessive moments due to the increased distance between its tip path plane and the centre of mass. Therefore the CCH model design features very stiff rotor blades that are spaced by 0.2R apart, with Table 1 showing the salient design features of the CCH rotor. In terms of the empennage design, the fin's chord is orientated so it is parallel with the fuselage's centreline. Generally, the fin is angled to offload the tail rotor at high speed but this is not required in the CCH model as the upper and lower rotors provide the torque balance.

Table 1. Main Rotor Design of the CCH and BL Models

Characteristic	Baseline Lynx	CCH
R	6.4m	5.49m
Ω	35.8 rad/s	40 rad/s
K_β	166352 Nm/rad	159240 Nm/rad
N_b	4	6
σ	0.077	0.153
γ	7.12	6.57
γ_s	3 deg	3 deg
I_β	678 kgm^2	450 kgm^2
θ_{tw}	-8.02 deg	-10 deg

Regarding the control of the CCH model, an extra control is introduced relative to the conventional helicopter. In the CCH model a differential collective control is introduced that allows the pilot to yaw the helicopter. The upper and lower rotor collectives take the form

$$\theta_u = \bar{\theta}_0 + \theta_{\text{diff}} \tag{5}$$

$$\theta_l = \bar{\theta}_0 - \theta_{\text{diff}} \tag{6}$$

Hence, a positive differential collective input increases the blade incidence of the upper rotor whereas it has the opposite effect on the lower rotor, having the net effect of yawing the helicopter's nose to the right. The tail rotor control is replaced by a differential control, θ_{diff}, and a propeller collective control, θ_{prop}, is also introduced resulting in a total of five controls thereby introducing control redundancy into the system. Therefore to trim the CCH model an extra state must be prescribed. Presently, the extra state is the pitch attitude as it directly impacts the thrust that the propeller is required to produce. One possibility is to set a fixed value of pitch to trim the helicopter at all flight speeds, for example $\theta = 0°$, fuselage level. However, this is not always desirable as it would require an excessive level of propeller thrust at certain flight speeds. Another concern is that in low speed flight there is no distinct advantage having the propeller providing thrust as it would unnecessarily increase the overall power consumption of the helicopter. Hence, rather than setting the pitch attitude to a fixed value for all flight speeds, a pitch schedule is developed to minimise the required propulsive force of the propeller. To obtain a pitch schedule the model is passed through an optimisation algorithm with Figure 5 showing the optimised pitch attitude and the propeller thrust to trim the CCH from hover up to 200 knots. The magnitude of the propeller thrust is very small until a speed of 60 knots meaning that the coaxial rotor is required to provide the propulsive thrust below 60 knots. However, after 60 knots the coaxial rotor's propulsive duties are shifted to the propeller, with 8 kN of thrust required at 200 knots. This optimisation result aids the design of the propeller with Table 2 showing the chosen design parameters of the propeller. The rotational speed is chosen to provide a high

velocity airflow over the propeller blades without compressibility effects becoming an issue at high speeds. The propeller also features Clark Y aerofoils along the span with a high level of twist so that each propeller blade element operates at a favourable angle of attack (Ref. 31).

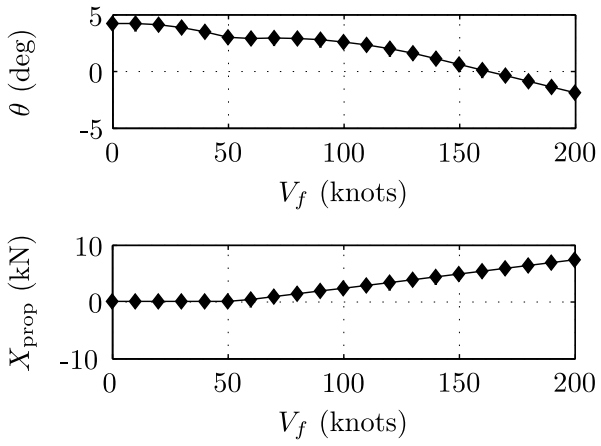

Fig. 5. Optimisation of the CCH Model

Trim Results of the Coaxial Compound Helicopter

Figure 6 shows the trim results of the CCH and BL models. In the hover, the coaxial inflow model, equations (1) and (2), result in higher induced velocities through the lower rotor than that of the upper rotor. Therefore, the induced power loss of the lower rotor is greater than the upper rotor, if the upper and lower thrust coefficients are equal. Hence, to provide a torque balance the upper rotor must create more thrust than the lower rotor to match the lower rotor's torque, with the thrust sharing ratio of the upper and lower rotors being 1.32 in the hover. Another consequence of the higher induced velocities of the lower rotor is the reduced blade incidence of the lower rotor blades if $\theta_u = \theta_l$. Therefore to compensate for the strong inflow through the lower rotor, the lower rotor's collective is slightly higher than that of upper rotor in low speed flight. This partitioning of the rotor thrusts and the higher pitch of the lower rotor are both consistent with findings from other trimmed coaxial rotors in hover (Refs. 22,32,33). As the CCH model moves away from hover the thrust sharing ratio tends towards unity and θ_{diff} tends towards zero as the aerodynamic interference between the rotors lessen as μ begins to dominate the coaxial inflow equations (1) and (2).

Another interesting feature of the trim results is the difference between the lateral cyclic required for both models. In a conventional helicopter a large amount of lateral cyclic is required between 0 - 50 knots, as can be seen with the BL model. As the conventional helicopter moves into forward flight the rotor wake skews backwards lowering blade incidence at the rear of the rotor disc. This effect causes the helicopter to roll to starboard (for a helicopter rotor that rotates anti-clockwise when viewed from above). In order to counteract this rolling moment a large amount of lateral cyclic is required to trim the helicopter. This effect still exists in the coaxial rotor but the two rotors flap in opposite directions requiring little lateral cyclic. For speeds above 150 knots, the propeller produces the majority of the axial thrust causing θ_{1c} to become negative to balance the propeller torque. The lack of tail rotor and the fin not being angled relative to the fuselage centreline reduces the side force that the helicopter produces from hover to 200 knots which consequently reduces the bank angle of the fuselage significantly. There is little difference between two longitudinal cyclic results (negative longitudinal cyclic tilts the rotor disc forward) until a flight speed of approximately 80 knots. After this flight speed the propeller begins to provide axial thrust reducing the longitudinal cyclic required.

Table 2. Propeller Design of the CCH Model

Design Parameter	CCH
R_{prop}	1.4m
Ω_{prop}	207 rad/s
θ_{tw}	-30 deg
σ_{prop}	0.142
$\mathbf{x}_{prop}$	(-7.66, 0, 0)m

HYBRID COMPOUND CONFIGURATION

Preliminary Design of the Hybrid Compound Helicopter

The HCH model features both wing and thrust compounding with the two propellers fulfilling the dual purpose of providing the anti-torque moment and propulsive thrust whereas the wing offloads the main rotor at high speeds. Like the CCH model, it is necessary to take into account some design considerations. The main design task is the sizing of propellers and wing. The addition of a wing to any compound helicopter configuration degrades hover performance by creating aerodynamic download and additional structural weight. The download and extra weight must be compensated with an increase in rotor thrust and an increase in power consumption. To retain good VTOL capability the wing must be sized in a manner that does not adversely reduce hover performance whilst having the ability to offload the main rotor at high speeds.

Another complication is that the sizing of the wing influences the design of the propellers. As mentioned previously, the propellers are required to provide the anti-torque moment in low speed flight. The propellers are mounted on the outer sections of the wing to provide adequate clearance between the propeller blades and the fuselage. It is clear that a greater wing span will result in lower propeller thrusts required to provide the anti-torque moment as the lever arm from the propeller to the centre of mass is increased. The selected wing area for the HCH model is $12m^2$ with an aspect ratio of 6. This wing area can create a significant amount of lift at high speed without adversely degrading hover performance. Also this combination of the wing area and aspect ratio creates a sizeable lever arm between the propellers and the centre of

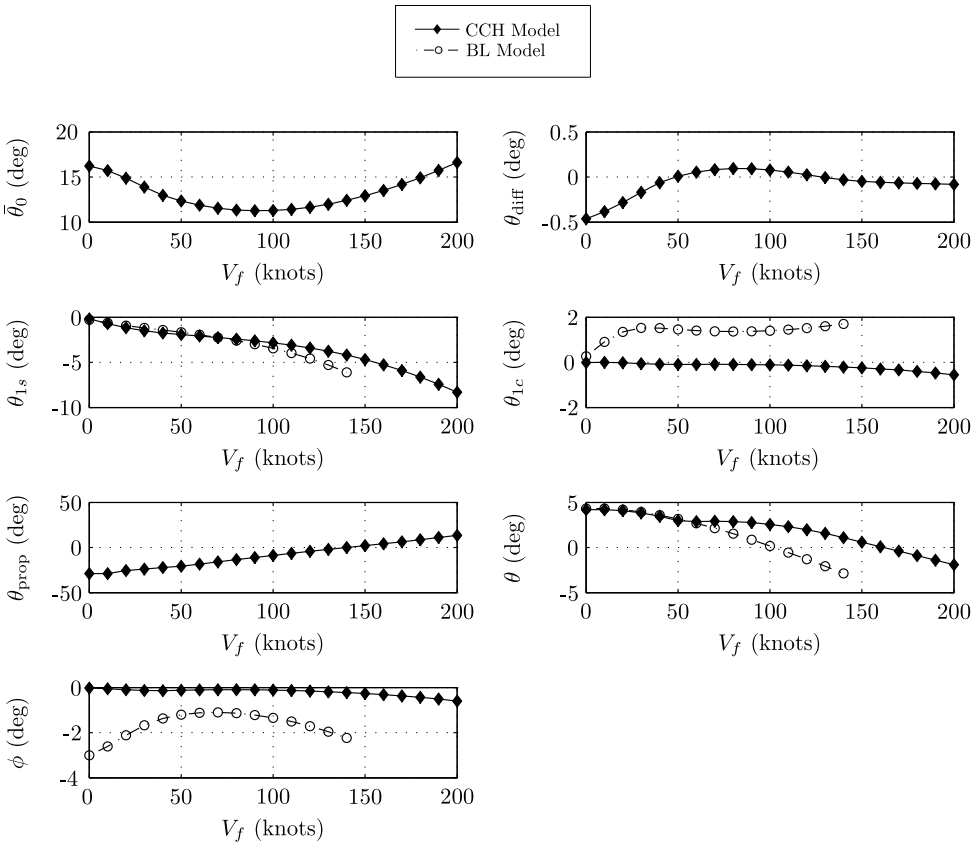

Fig. 6. Trim Results of the CCH Model

mass thus reducing the propeller thrusts at low speed flight. In terms of the aspect ratio, a value of 6 is chosen because a higher aspect ratio would lead to a wing span that would extend further into the higher velocities of the rotor wake whereas a lower aspect ratio would result in a greater induced drag penalty (Ref. 34). A choice of 6 is an appropriate compromise between these two effects and has been used on various winged helicopters (Refs. 10, 35). Also the moment of inertia around the x axis, I_{xx}, has been slightly increased to account for the offset mass of the wing from the centre of gravity.

Concerning the control of the HCH model, a mean propeller collective setting controls the magnitude of the two propeller thrusts whereas a differential propeller collective controls the yawing motion of the helicopter. The starboard and port propeller collectives take the from

$$\theta_{\text{star}} = \bar{\theta}_{\text{prop}} + \theta_{\text{diff}} \tag{7}$$

$$\theta_{\text{port}} = \bar{\theta}_{\text{prop}} - \theta_{\text{diff}} \tag{8}$$

The differential propeller setting, θ_{diff}, mean propeller collective, $\bar{\theta}_{\text{prop}}$, as well as the standard main rotor collective and cyclic controls result in five controls. As with the CCH model the extra state that is controlled is the pitch attitude. In this design controlling the pitch attitude is particularly useful as it allows for direct control of the wing lift. In a similar manner to the CCH model, the model is passed through an optimisation algorithm to develop a pitch schedule for the HCH model that reduces the required propeller thrusts. It should be noted that the HCH model could, in theory, be trimmed with a pitch attitude of zero at all flight speeds but there is an important issue that arises in low speed flight. In order to trim the HCH model in the hover, at a pitch attitude of zero, a large amount of negative thrust is required from the port propeller. As forward speed increases and the port propeller continues to create large amounts of negative thrust, to maintain a level fuselage, the forward velocity and the induced velocity of the port propeller travel in opposite directions. When their magnitudes are similar there would be no well defined slipstream and eventually the vortex ring state would be reached at some flight speed, resulting in the solutions from momentum theory being no longer valid (Ref. 36). Hence the pitch attitude is scheduled in such a manner that avoids the port propeller providing large amounts of negative thrust in low speed flight. Figure 7 shows the pitch schedule and propeller thrusts that are required from hover up to a flight speed of 150 knots. This manner of pitch scheduling does impose the penalty of increasing the pitch attitude in the hover, from 4.3° for the BL model to 8.4° for the HCH model. The reason for this increase in pitch attitude is that the starboard propeller provides a significant thrust to provide the anti-torque moment and the main rotor flaps backwards to oppose this force. For the trim

problem, the pitch attitude is set close to zero after 150 knots to maximise the lift produced by the wing. A combination of setting the pitch attitude to zero after 150 knots as well as a fixed wing pitch setting of 5° maximises the lift of the wing whilst maintaining an adequate stall margin. Again, the optimisation results aid the propellers design by showing the thrusts required. The starboard and port propellers are identical with the exception that they rotate in opposite directions with Table 3 showing the important design properties of the propellers.

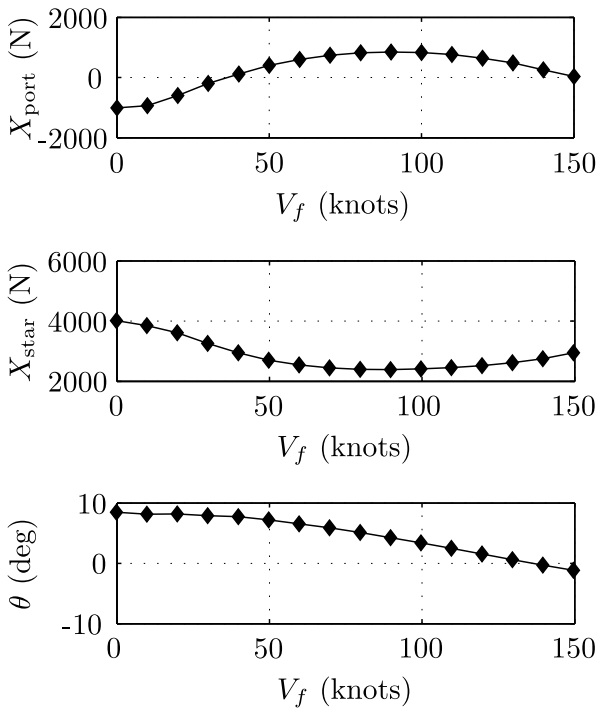

Fig. 7. Optimisation Results of the HCH Model

Trim Results of the Hybrid Compound Helicopter

The trim results of the HCH model and the BL model are shown in Figure 8. The first result to note is the difference between the collective settings. As the speed approaches 50 knots, the collective setting of the HCH model begins to reduce as the wing begins to offload the main rotor whereas with the BL model the collective begins to increase tending towards the limiting case of retreating blade stall. There is little difference between the longitudinal cyclic of the two models until 80 knots. However, after 80 knots, the two propellers begin to supply the propulsive force and therefore the rotor disc is no longer required to be tilted forward to provide the propulsive force. There is less lateral cyclic required in the hover due to the rotor not having to produce a side force to counteract the tail rotor. At higher speeds the lateral cyclic required is less than that of the BL model due to wing offloading the main rotor. For the BL model, at high speeds, there is a natural tendency of the rotor to tilt to the advancing side due to the coning of the rotor (Ref. 37). However, for the HCH model, the coning of the rotor is reduced which slightly lowers the lateral cyclic required to balance the rolling moment. The lack of tail rotor also reduces the bank angle of the fuselage for all flight speeds. The differential propeller collective is at its highest in low speed flight to provide the anti-torque moment. As forward speed increases, the anti-torque moment duties are shifted towards the fin as it provides a side force which results in the propeller differential setting lowering as speed increases.

Table 3. Propeller Design of the HCH Model

Design Parameter	HCH
R_{prop}	1.3m
Ω_{prop}	207 rad/s
θ_{tw}	-30 deg
σ_{prop}	0.153
$\mathbf{x}_{prop}$	(0.05, $\pm$3.87, 0.13)m

Figure 9 compares the trim results of the CCH and HCH models. The main rotor collective of the CCH model is of similar form to a conventional helicopter. Whereas the collective of the HCH model lowers after 50 knots due to the wing offloading the main rotor. The longitudinal cyclic of the two models are similar until a flight speed of 100 knots. However, after 100 knots, the longitudinal cyclic of the HCH model is less due to two propellers providing the majority of propulsive force. With the CCH model, at high speeds, there is only one propeller providing additional axial thrust and therefore to trim the helicopter the main rotor and propeller combine to provide the propulsive force which requires the rotor disc to tilted more forward. The form of lateral cyclic of the HCH model is similar to that of a conventional helicopter whereas with the CCH model the lateral cyclic required is very small due to the coaxial rotor arrangement. In terms of the propeller controls, both are very similar and linear with flight speed. Concerning the pitch attitudes of the two helicopters, the pitch attitude of the HCH model is higher than the CCH model in low speed flight as the main rotor flaps back to oppose the starboard propeller thrust that provides the anti-torque moment. With the CCH model, in low speed flight the pitch attitude is similar to a conventional helicopter as the propeller does not produce any meaningful axial thrust. The roll angle of the CCH model is very small at all flight speeds as the empennage design produces little side force in trim as the coaxial rotor system provides the torque balance. Whereas the roll angle of the HCH model is slightly higher than the CCH model due to the side force that the fin produces.

DYNAMIC STABILITY OF THE TWO COMPOUND CONFIGURATIONS

The two compound helicopter models have been trimmed and the next logical step is assessing their dynamic stability. All the helicopter models that are presented within the paper take the non-linear form of

$$\dot{\mathbf{x}} = \mathbf{f}(\mathbf{x}, \mathbf{u}) \tag{9}$$

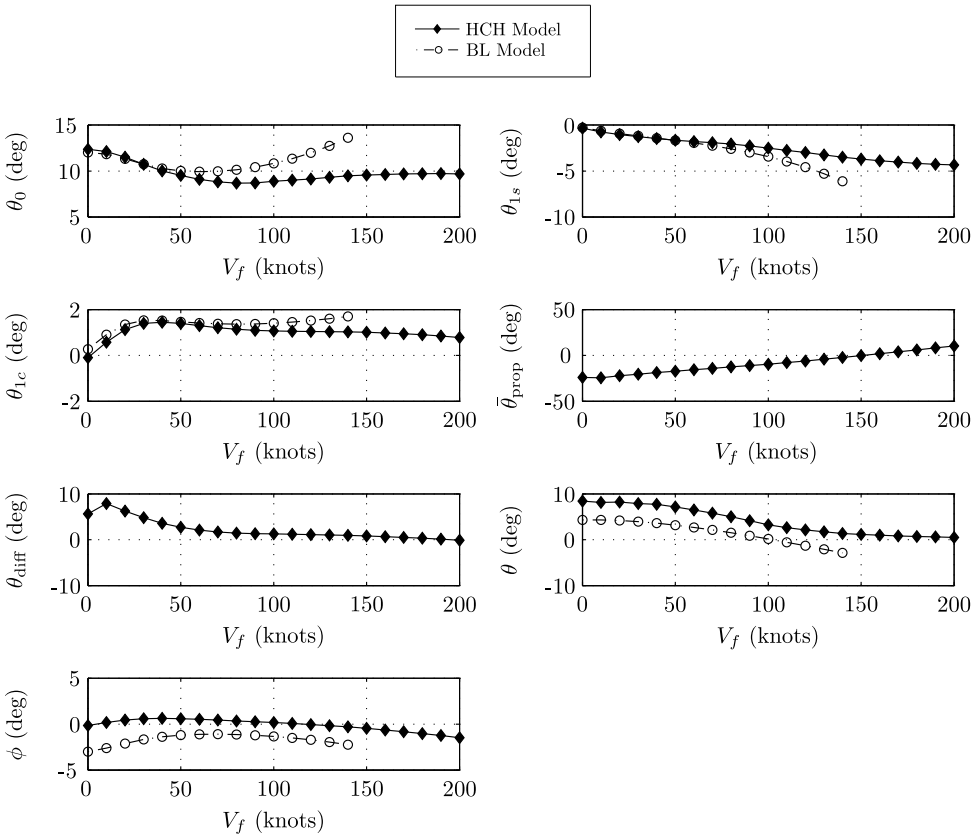

Fig. 8. Trim Results of the HCH Model

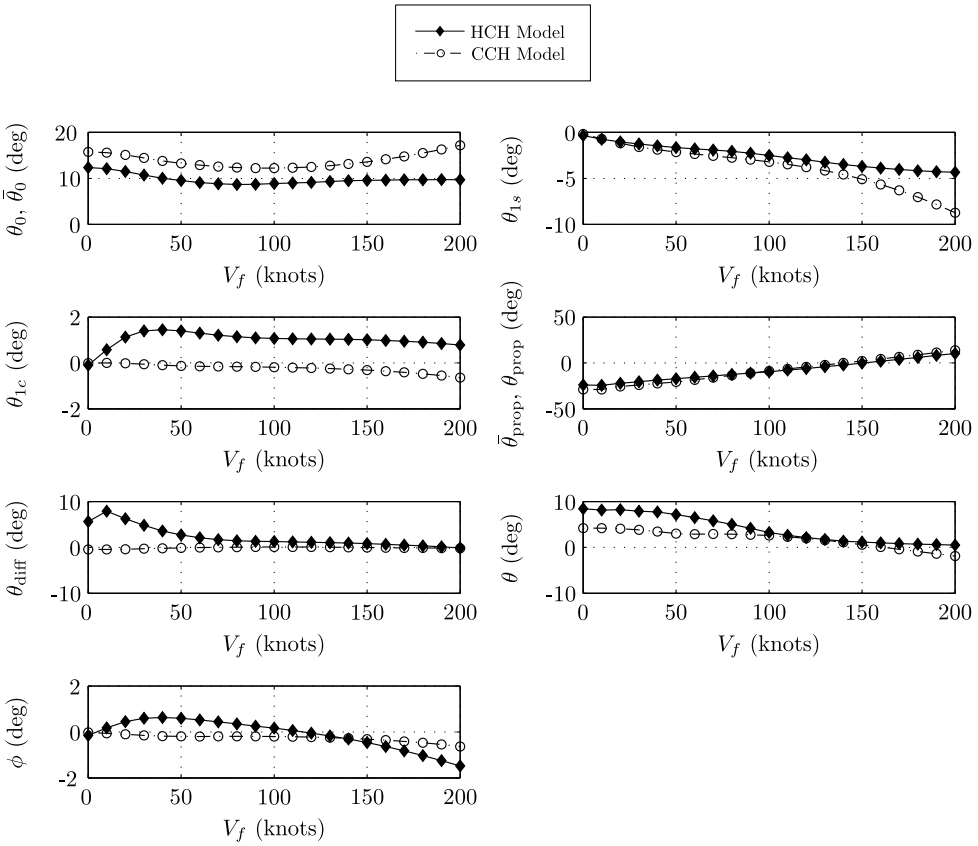

Fig. 9. Trim Results of the HCH and CCH Models

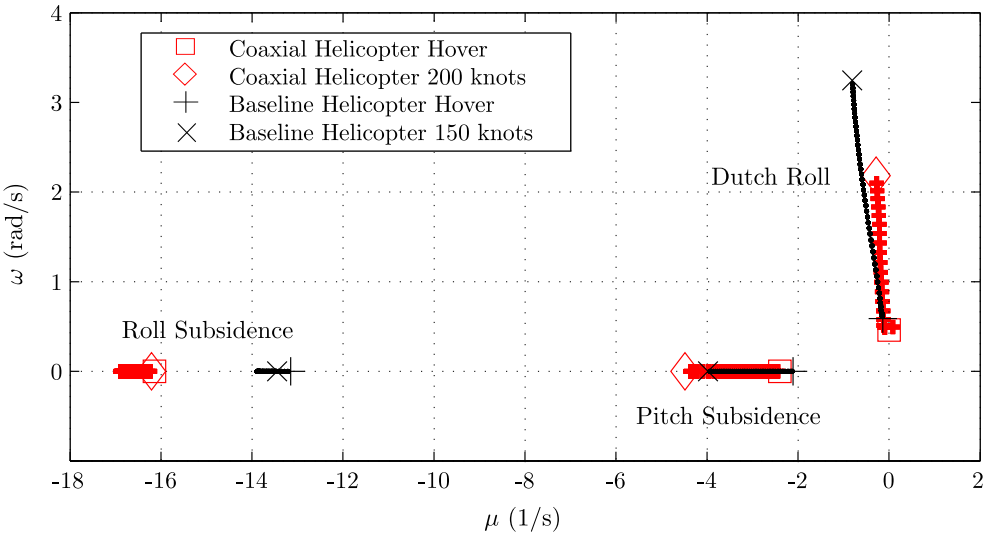

Fig. 10. Roll Subsidence, Pitch Subsidence and Dutch Roll Modes Modes of the CCH and BL Models

Using small perturbation theory, equation (9) can be reduced to the linearised form of

$$\dot{\mathbf{x}} = \mathbf{A}\mathbf{x} + \mathbf{B}\mathbf{u} \tag{10}$$

where **A** and **B** are known as the stability and control matrices. Due to the complex nature of the non-linear equations of motion for these helicopters the equations are reduced to linear form using a numerical linearisation algorithm (Ref. 38). Using this technique the stability and control matrices can be formed at various trimmed conditions. Furthermore, the eigenvalue values of the stability matrix give the natural modes of motion at that particular flight condition. Using these techniques, a dynamic stability analysis of each compound helicopter is performed from hover to 200 knots.

Dynamic Stability of the CCH Model

Figure 10 shows the roll subsidence, pitch subsidence and dutch roll modes of both the BL and CCH models. All three of these modes exhibit stability for both helicopter models. The damping of the roll subsidence mode of the CCH model has increased slowing the roll response of the aircraft. The reason for this is due to a combination of the increased number of rotor blades, their stiffness and the increased distance between the upper rotor's hub and the centre of gravity. The level of roll damping is given by L_p and for the CCH model is insensitive to flight speed with it being approximately -15 $(1/s)$.

In terms of the dutch roll mode, the main difference is the frequency of the two modes, with the CCH model exhibiting a smaller frequency, at high speeds, due to its empennage design. This can be seen by using Padfield's (Ref. 17) approximation to the dutch roll mode frequency in high speed flight

$$\omega_{\text{dr}}^2 \approx U_e N_v + L_v \left(\frac{g - N_p U_e}{L_p} \right) \tag{11}$$

The reduced dutch roll frequency of the CCH model is due to the Weathercock stability derivative N_v. For a conventional helicopter N_v is generally positive for most flight speeds with the tail rotor and fin playing the most prominent roles. Following a sideslip perturbation the fin and tail rotor provide a side force that aligns the fuselage nose with the wind direction, thus providing a stabilising effect. However, for the CCH model this derivative is actually destabilising for all flight speeds due to the combination of the lack of tail rotor and the fin not being angled relative to the fuselage centreline. These two design features reduce the yawing moment that the helicopter produces following a sideslip perturbation. The fuselage is now the main contributor to N_v which provides a destabilising moment following a sideslip perturbation due to the fuselage's aerodynamic centre being located fore of the centre of gravity position. In forward flight, equation (11) shows that a negative value of N_v reduces the dutch roll frequency which can be seen in Figure 10.

Figure 11 shows the phugoid, heave subsidence and spiral modes of the BL and CCH models. The phugoid mode for both the BL and CCH models are of similar form and exhibit instability for all flight speeds. These two models feature hingeless rotor systems and this is the primary reason for the instability (Ref. 39). The stiff rotors create large moments around the rotor hub due to the stiffness of the blades and large effective hinge offset. When the two helicopters are subject to a perturbation in forward speed, the two rotor systems flap backwards resulting in the fuselage pitching up. As the fuselage pitches up, the stability derivative M_q provides a pitch down moment with this oscillatory motion continuing with the amplitude steadily increasing. The phugoid mode of the CCH model comes close to the imaginary axis, between 50 - 80 knots, due to an increase in drag damping. Following a perturbation in forward speed the blade incidence of the propeller blades reduce providing an extra drag force, lowering the value of X_u, but this is still insufficient to stabilise the

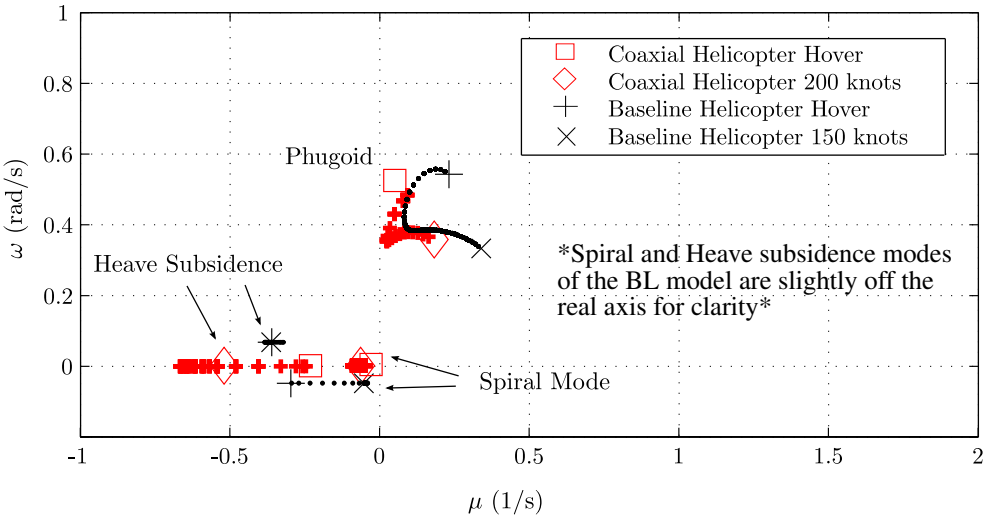

Fig. 11. Heave Subsidence, Phugoid and Spiral Modes of the CCH and BL Models

phugoid. The eigenvalues of the spiral mode for two models are small and negative indicating stability for both the models. The spiral mode of the CCH model is insensitive to flight speed whereas flight speed has more influence with regards to the BL model's spiral mode.

Dynamic Stability of the HCH Model

Figure 12 shows the heave subsidence, roll subsidence, pitch subsidence and dutch roll modes of both the BL and HCH models. Firstly, consider the roll subsidence mode. For the BL model the roll damping does not change significantly from hover to 150 knots and is dominated by the stiffness of the rotor. However, the roll damping eigenvalues of the HCH model range from -9.5 $(1/s)$ in the hover to -14 $(1/s)$ at 200 knots. In the HCH model the structural weight of the wing creates a greater moment of inertia around the x axis than that of the BL helicopter. Although the stiffness properties remain the same for these two helicopter rotors the HCH model's roll damping is scaled by I_{xx} thus resulting in a lower value of L_p in the hover. As speed increases the lift produced by the wing increases and the damping of the roll mode also increases. At high speeds, the wing is producing a significant portion of the overall lift of the helicopter. In a fixed wing aircraft the roll mode is always stable as a positive perturbation in roll rate increases the angle of attack of the starboard wing and decreases the angle of attack of the port wing (Ref. 40), thus producing a stabilising rolling moment. This effect also occurs in the HCH model and is now added to the roll damping produced by the hingeless rotor.

Another notable result from Figure 12 is the increase in damping of the heave subsidence mode and the decreased damping of the pitch subsidence mode of the HCH model. The change of these two modes is primarily due to the stability derivatives Z_w and M_w. Padfield (Ref. 17) approximates the characteristic equation of the short period modes as

$$\lambda_{sp}^2 - (Z_w + M_q)\lambda_{sp} + Z_w M_q - M_w(Z_q + U_e) = 0 \qquad (12)$$

In terms of the HCH model, at high speeds, the stability derivatives Z_w and M_w both decrease, relative to the BL model. The former decreases because there are now two main sources of lift: the main rotor and wing. Therefore a positive perturbation of angle of attack, α, increases the rotor thrust and the lift of the wing resulting in a greater total lifting force. The attack of angle stability derivative M_w also decreases due to the wing. The quarter chord position of the wing is slightly aft of the centre of gravity position. Therefore, after a perturbation in normal velocity the wing produces a negative pitch down moment which opposes the main rotor contribution to M_w. This combination creates a cancelling effect between the main rotor and the wing which results in M_w becoming very close to zero at 200 knots. If M_w is assumed to zero at high speeds, then the solutions of equation (12) are

$$\lambda_{sp} \approx M_q \qquad (13)$$
$$\lambda_{sp} \approx Z_w \qquad (14)$$

At 200 knots, for the HCH model M_q = -2.7 $(1/s)$ and Z_w = -1.5 $(1/s)$, which agree favourably with the eigenvalues presented in Figure 12, with the derivative Z_w capturing the heave subsidence mode whereas M_q estimates the pitch damping mode. The net effect of the change of these two derivatives is that their eigenvalues become closer together at high speeds.

Figure 13 shows the phugoid and spiral modes of the HCH and BL models. In the hover, the phugoid modes of the HCH and BL models are similar. However, as speed increases the mode becomes stable for the HCH model but with decreasing frequency. Therefore the phugoid tends towards an exponential mode rather than the oscillatory mode of the BL model.

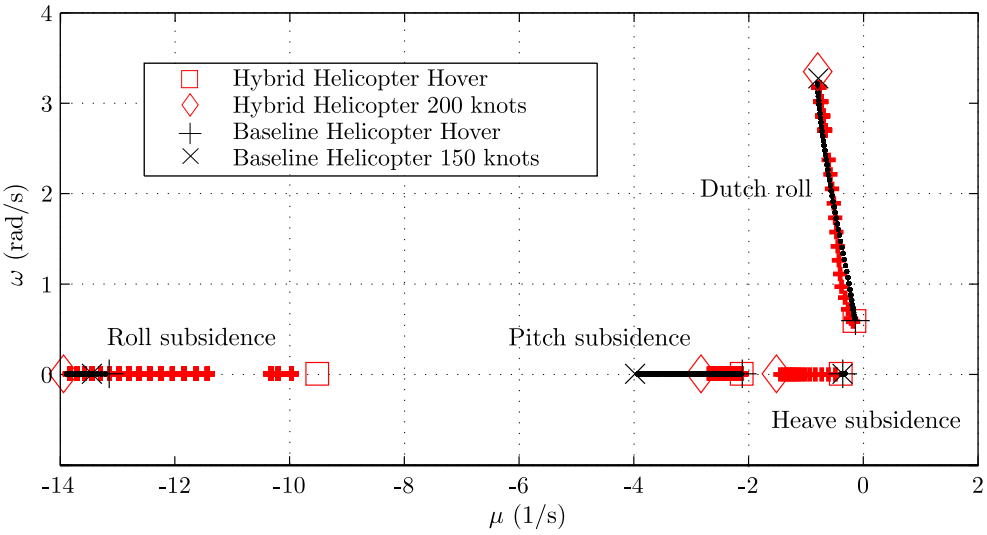

Fig. 12. Heave Subsidence, Roll Subsidence, Pitch Subsidence and Dutch Roll Modes of the HCH and BL Model

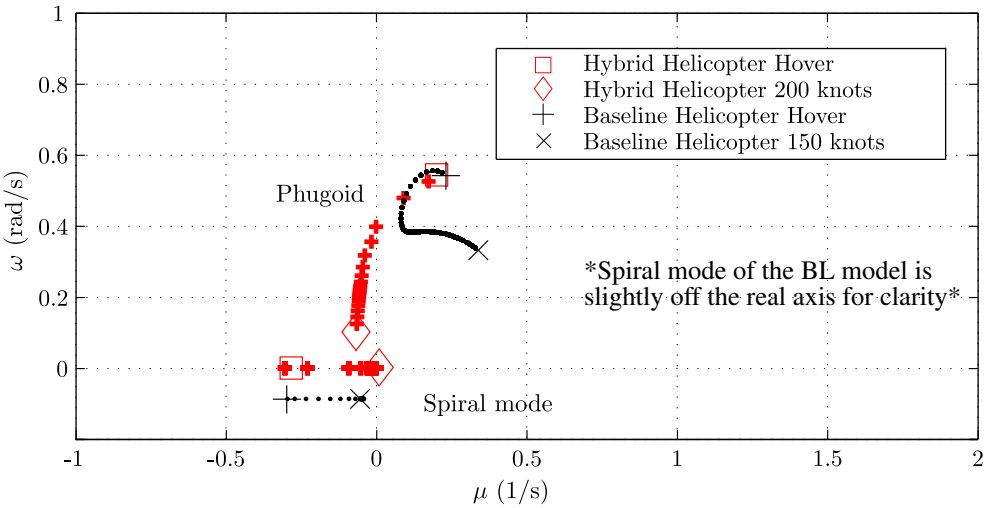

Fig. 13. Phugoid and Spiral Modes of the HCH and BL Model

The oscillatory nature of the mode is reduced due to the contribution of M_u with this derivative tending towards zero above 160 knots. This derivative is analogous to M_w with the wing providing a cancellation of the pitch up moment produced by the main rotor following a perturbation of forward speed. The net effect is that the ratio of the pitching moment due to speed and pitch rate becomes very small lessening the oscillatory nature of the phugoid. Care must be taken to ensure this mode does not branch off into the real axis and eventually produce a purely divergent motion. Concerning the damping of the mode, after 40 knots the phugoid becomes stable due to the drag damping derivative, X_u. For a conventional helicopter X_u is always negative as a perturbation in forward velocity results in an increase in drag force due to the fuselage and the rotor disc tilting backwards. However, for the HCH model, the drag is increased following a perturbation in forward velocity due to the addition of the two propellers and wing. A perturbation in forward velocity reduces the blade incidence of the propeller blades which creates a sizeable drag force. Additionally, the perturbation of u also increases the drag of the wing, hence both contribute to lower the drag damping derivative, X_u, which in turn stabilises the phugoid.

Figure 14 shows the comparison between the roll subsidence, pitch subsidence, heave subsidence and dutch roll modes of the CCH and HCH models. The roll damping of the CCH model is insensitive to flight speed whereas the flight speed has a profound influence with regards to damping of the HCH model. The roll damping of the HCH model is at its lowest in the hover and increases with flight speed due to the wing providing a large portion of the vehicle lift. Regarding the dutch roll modes, both models predict a lightly damped mode with the main difference being the frequencies of the two modes. As for the short period modes, the eigenvalues of the HCH model's heave and pitch subsidence modes are ap-

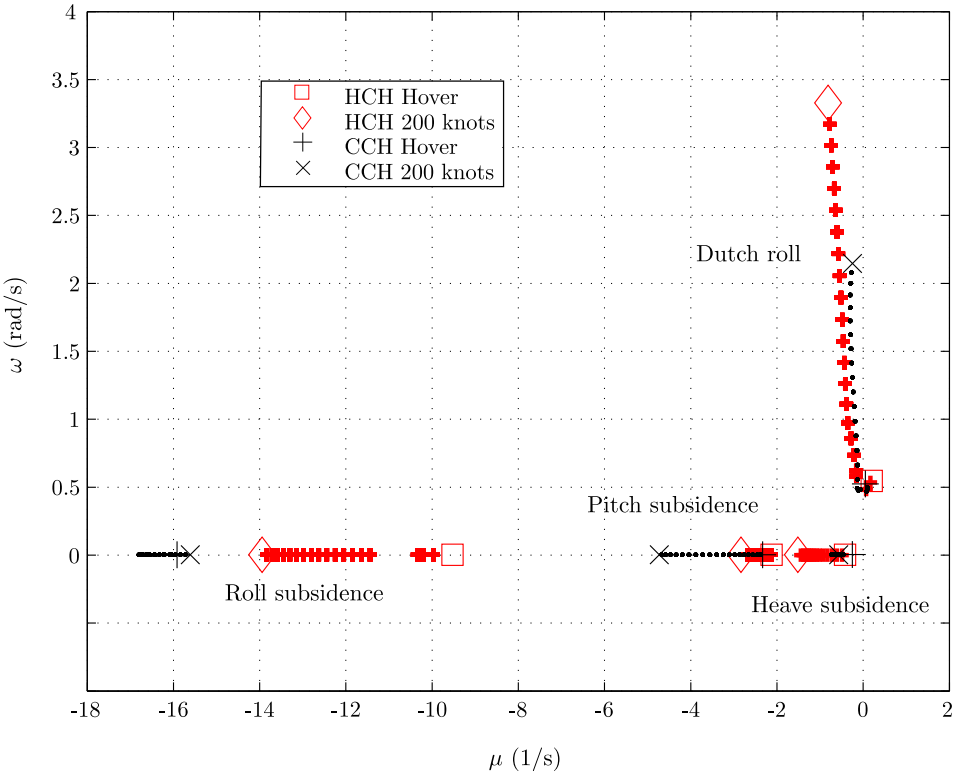

Fig. 14. Heave Subsidence, Roll Subsidence, Pitch Subsidence and Dutch Roll Modes of the CCH and HCH Models

proximated with equations (13) and (14). For a conventional helicopter in high speed flight, the derivative M_w influences the eigenvalues of the short period modes, as seen in equation (12). However, for the HCH model, M_w is very small due to the wing's contribution following a perturbation of angle of attack resulting in Z_w and M_q determining the damping of the heave and pitch subsidence modes, respectively. With regards to the CCH model, the stability derivative M_w becomes increasingly significant at high speeds influencing the heave and pitch subsidence modes. Similar to that of the BL model, the contribution of M_w results in the heave and pitch subsidence eigenvalues being well separated throughout the speed range.

Figure 15 shows the phugoid and spiral modes of the CCH and HCH models. The phugoid mode of the HCH model becomes stable after 40 knots due the increased drag following a perturbation of forward speed. However, the oscillatory nature of the mode is reduced due to the wing providing a stabilising moment following a perturbation of forward velocity. Whereas the form of the phugoid mode of the CCH model is similar to that of the BL model due the speed stability derivative M_u. For the CCH model, M_u is positive for all flight speeds as a perturbation of forward speed results in the rotor disc flapping backwards thus producing a pitching up motion. The propeller of the CCH model does contribute to reduce the drag damping derivative X_u, but its contribution is incapable of stabilising the phugoid. In relation to the spiral modes, the eigenvalues are small and negative for all flight speeds indicating stability for the two models.

CONCLUSIONS

Two compound helicopter models have been developed and their trim and dynamic stability has been compared to a conventional helicopter. The main conclusions from the current work are as follows:

1. A coaxial rotor model has been developed and has been partially validated with experimental results. The results show good agreement in the hover and at high speed flight but due to a lack of experimental data a full validation is still not yet completed.

2. The trim results of the CCH model show that little lateral cyclic control is required to trim the helicopter. Also the omission of a tail rotor in the design significantly reduces the bank angle of the fuselage across the speed range.

3. The trim results of the HCH model show a reduction of collective required after 50 knots as the wing begins to offload the main rotor. The differential propeller collective control required is at its highest in low speed flight but reduces as flight speed increases as the fin provides the anti-torque moment. There is also less longitudinal cyclic required after 80 knots as the propellers provide the propulsive force.

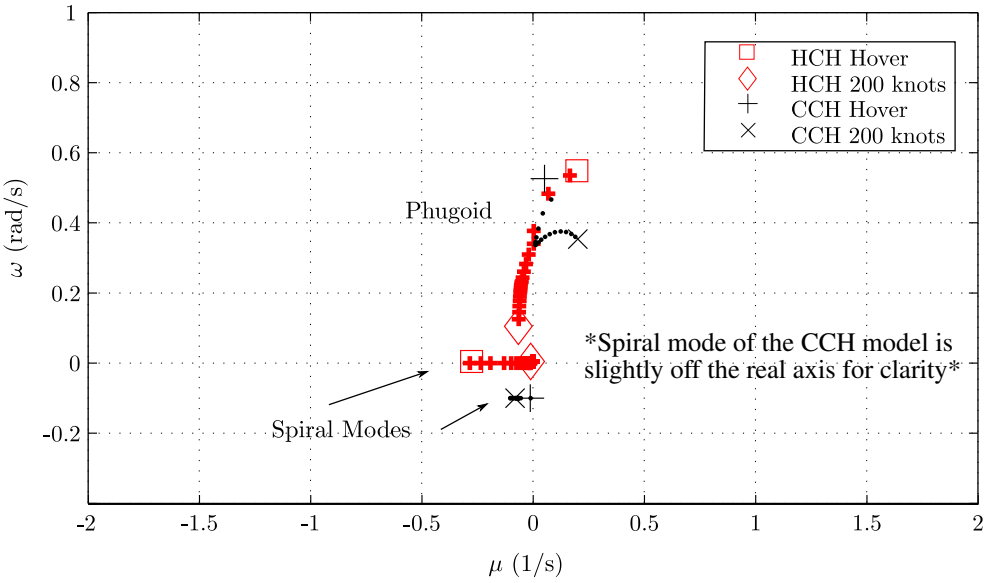

Fig. 15. Phugoid and Spiral Modes of the CCH and HCH Models

4. The main differences between the natural modes of motion of the CCH and BL models are the dutch roll and roll subsidence modes. The frequency of the dutch roll mode is less than that of the BL mode due to the lack of tail rotor and a reduced side force contribution from the fin, following a sideslip perturbation. The differences between the roll modes is primarily due to the design of the main rotor systems. The increased number of rotor blades, their respective stiffness and the increased distance between the upper rotor's hub to the centre of gravity position all contribute to increasing the roll damping, relative to the BL model.

5. The main differences between the HCH and BL modes of motion were the phugoid and heave subsidence modes. There is an increase in heave damping with the HCH model due to the main rotor and wing both providing a greater lifting force following a perturbation of angle of attack. The phugoid becomes stable for the HCH model due to the increase in drag damping, the lowering of X_u, however the mode tends towards an exponential response due the cancelling effect of pitching moments between main rotor and wing. This is because the wing provides a pitch down moment following a perturbation in angle of attack since its quarter chord position is slightly behind the centre of mass. Therefore, the positioning of the wing can strongly influence the phugoid mode of the helicopter.

This paper has investigated the dynamic stability of compound helicopter configurations, however it must be stressed that more work has to be done to fully investigate the compound configuration. One area for future work relates to the control of the compound helicopter and how the additional control(s) could be utilised during standard helicopter manoeuvres to maximise performance. This would naturally lead to a handling qualities assessment of these aircraft and how the pilot workload is affected by this additional control. These studies would assist the design of the compound helicopter and could perhaps reinforce the potential of the compound helicopter.

REFERENCES

[1]Orchard, M., "The compound helicopter - why have we not succeeded before?" *The Aeronautical Journal*, Vol. 103, (1028), pp. 489–495.

[2]Leishman, J., *Principals of Helicopter Aerodynamics*, Cambridge University Press, second edition, 2006.

[3]Burgess, R., "The ABC Rotor - A Historical Perspective," American Helicopter Society 60th Annual Forum, 2004.

[4]Bagai, A., "Aerodynamic Design of the X2 Technology Demonstrator Main Rotor Blade," 64th Annual Forum of the American Helicopter Society, 2008.

[5]Blackwell, R. and Millott, T., "Dynamics Design Characteristics of the Sikorsky X2 Technology Demonstrator Aircraft," American Helicopter Society 64th Annual Forum, 2008.

[6]Walsh, D., Weiner, S., Bagai, A., Lawerence, T., and Blackwell, R., "Development Testing of the Sikorsky X2 Technology Demonstrator," 65th Annual American Helicopter Forum, 2009.

[7]Arcidiacono, P., DeSimone, G., and Occhiato, J., "Preliminary Evaluation of RSRA Data Comparing Pure Helicopter, Auxiliary Propulsion and Compound Helicopter Flight Characteristics," 36th Annual National Forum of the American Helicopter Society, 1980.

[8]Lentine, F., Groth, W., and Oglesby, T., "Research in Maneuverability of the XH-51A Compound Helicopter," USAAVLABS Technical Report 68-23, 1968.

[9]Prouty, R., "The Lockheed Helicopter Experience," 65th Annual American Helicopter Forum, 2009.

[10]Dumond, R. and Simon, D., "Flight Investigation of Design Features of the S-67 Winged Helicopter," 28th Annual Forum National Forum of the American Helicopter Society, 1972.

[11]Orchard, M. and Newman, S., "The fundamental configuration and design of the compound helcopter," *Proceedings of the Institution of Mechanical Engineers, Part G: Journal of Aerospace Engineering*, Vol. 217, (6), 2003, pp. 297–315.

[12]Sekula, M. and Gandhi, F., "Effects of Auxiliary Lift and Propulsion on Helicopter Vibration Reduction and Trim," *Journal of Aircraft*, Vol. 41, (3), 2004, pp. 645–656.

[13]Prouty, R., *Helicopter Performance, Stability, and Control*, Robert E. Krieger Publishing Company, Inc., reprint edition, 1990.

[14]Orchard, M. and Newman, S., "Some design issues for the optimisation of the compound helicopter configuration," 56th American Helicopter Society Annual National Forum, 2000.

[15]Buhler, M. and Newman, S., "The Aerodynamics of the Compound Helicopter Configuration," *Aeronautical Journal1*, Vol. 100, 1996, pp. 111–120.

[16]Houston, S., "The Gyrodyne - A Forgotten High Performer?" *Journal of the American Helicopter Society*, Vol. 52, (4), 2007, pp. 382 – 391.
doi: http://dx.doi.org/10.4050/JAHS.52.382

[17]Padfield, G., *Helicopter Flight Dynamics*, Blackwell Science, 1996.

[18]Thomson, D., "Development of a Generic Helicopter Mathematical Model for Application to Inverse Simulation," Internal Report No. 9216, Department of Aerospace Engineering, University of Glasgow, UK, 1992.

[19]Leishman, J. and Syal, M., "Figure of Merit Definition for Coaxial Rotors," *Journal of the American Helicopter Society*, Vol. 53, (3), 2008, pp. 290–300.

[20]Leishman, J. and Ananthan, S., "An Optimum Coaxial Rotor System for Axial Flight," *Journal of the American Helicopter Society*, Vol. 53, (4), 2008, pp. 366–381.

[21]Kim, H. and Brown, R., "A Rational Approach to Comparing the Performance of Coaxial and Conventional Rotors," *Journal of the American Helicopter Society*, Vol. 55, (012003), 2010.

[22]Kim, H. and Brown, R., "A Comparison of Coaxial and Conventional Rotor Performance," *Journal of the American Helicopter Society*, Vol. 55, (012004), 2010.

[23]Paglino, V., "Forward Flight Performance of a Coaxial Rigid Rotor," Proceedings of the 27th American Helicopter Forum, 1971.

[24]Harrington, R., "Full-Scale-Tunnel Investigation of the Static-Thrust Performance of a Coaxial Helicopter Rotor," NACA TN-2318, 1951.

[25]Dingeldein, R., "Wind-Tunnel Studies of the Performance of Multirotor Configurations," NACA TN 3236, 1954.

[26]Bagai, A. and Leishman, J., "Free-Wake Analysis of Tandem, Tilt-Rotor and Coaxial Rotor Configurations," 51st Annual Forum of the American Helicopter Society, 1995.

[27]Sequeira, C. J., Willis, D. J., and Peraire, J., "Comparing Aerodynamic Models for Numerical Simulation of Dynamics and Control of Aircraft," 44th AIAA Aerospace Sciences Meeting and Exhibit, 2006.

[28]Lynn, R., "Wing- Rotor Interactions," *Journal of Sound and Vibration*, Vol. 4, (3), 1966, pp. 388–402.

[29]Arents, D., "An Assessment of the Hover Performance of the XH-59A Advancing Blade Concept Demonstration Helicopter," , 1977.

[30]Walsh, D., "High Airspeed Testing of the Sikorsky X2 Technology Demonstrator," 67th Annual Forum of the American Helicopter Society, 2011.

[31]Von Mises, R., *Theory of Flight*, Dover Publications, 1959.

[32]Zimmer, H., "The Aerodynamic Calculation of Counter Rotating Coaxial Rotors," 11th European Rotorcraft Forum, 1985.

[33]Lim, J., McAlister, K., and Johnson, W., "Hover Performance Correlation for Full-Scale and Model-Scale Coaxial Rotors," *Journal of the American Helicopter Society*, Vol. 54, 2009.

[34]Keys, C., "Performance Prediction of Helicopters," *Rotor-Wing Aerodynamics*, edited by W. Stepniewski, Dover Publications, Inc., 1981.

[35]Torres, M., "A Wing on the SA.341 Gazelle Helicopter and its Effects," *Vertica*, Vol. 1, 1976, pp. 67–73.

[36]Johnson, W., *Helicopter Theory*, Dover Publications, Inc., second edition, 1994.

[37]Watkinson, J., *The Art of the Helicopter*, Elsevier Butterworth-Heinemann, 2004.

[38]Stevens, B. and Lewis, F., *Aircraft Control and Simulation*, John Wiley and Sons, second edition, 2003.

[39]Bramwell, A., *Helicopter Dynamics*, Edward Arnold, first edition, 1976, p. 212.

[40]Cook, M., *Flight Dynamics Principles*, Elsevier Ltd., third edition, 2013.